

Charge Efficiency of Ni/H₂ Cells During Transfer Orbit of Telstar 4 Satellites

by

W.C. Fang, D.W. Maurer, B. Vyas and M.N. Thomas

INTRODUCTION

The TELSTAR 4 communication satellites being manufactured by Martin Marietta Astro Space (Astro Space) for AT&T are three axis stabilized spacecraft¹ scheduled to be launched on expendable vehicles such as the Atlas or Ariane rockets. Typically, these spacecraft consist of a box that holds the electronics and supports the antenna reflectors and the solar array wings. The wings and reflectors are folded against the sides of the box during launch and the spacecraft is spun for attitude control in that phase; they are then deployed after achieving the final orbit. The launch phase and transfer orbits required to achieve the final geosynchronous orbit typically take 4 to 5 days during which time the power required for command, telemetry, attitude control, heaters, etc., is provided by two 50 AH nickel hydrogen batteries augmented by the exposed outboard solar panels. In the past, this situation has presented no problem since there was a considerable excess of power available from the array.

In the case of large high powered spacecraft such as TELSTAR 4, however, the design power levels in transfer orbit approach the time-averaged power available from the exposed surface area of the solar arrays, resulting in a very tight power margin. To compound the difficulty, the array output of the spinning spacecraft in transfer orbit is shaped like a full wave rectified sine function and provides very low charging rates to the batteries during portions of the rotation (Fig 1). In view of the typically low charging efficiency of alkaline nickel batteries at low rates, it was decided to measure the efficiency during a simulation of the TELSTAR 4 conditions at the expected power levels and temperatures on three nickel hydrogen cells of similar design. The unique feature of nickel hydrogen cells that makes the continuous measurement of efficiency possible is that hydrogen is one of the active materials and thus, cell pressure is a direct measure of the state of charge or available capacity. The pressure is measured with a calibrated strain gage mounted on the outside of the pressurized cell.

¹The spacecraft is actually spin stabilized in transfer orbit and three axis stabilized (sometimes called body stabilized) on station in the earth centered coordinate system using momentum wheels and magnetic torquers.

PRECEDING PAGE BLANK NOT FILMED

SIMULATION PARAMETERS

The array power was calculated in one degree increments of spacecraft rotation and the expected stowed array output. The efficiencies of the charge and discharge converters were in excess of 90%. The resulting battery charge or discharge current is shared by the two batteries for each degree of rotation. These calculations were performed for various spacecraft (S/C) power levels up to 490 W which represents the expected load with active transfer orbit equipment; also covered were lower loads (430W) such as those available after the LAE burns, etc.

Traditionally, both batteries share the charge and discharge currents equally (parallel operation) so that the net time-averaged charging current, with 430 W S/C load, is only $C/98$. At 490W S/C load the situation would be much worse. A practical solution was to employ "sequential charging" to increase the charging current. In this mode, all the charge current is fed into one battery with the other left on open circuit during the charge phase; after a period of time, e.g. 15 minutes, the batteries are switched. In this case, the charging efficiency increases to well above 90% for the 430W load (Fig.2). Precise measurements of the charge efficiency during sequential charging under simulated transfer orbit cycle power conditions are presented in this study.

EXPERIMENT

The transfer orbit cycle simulation was accomplished by utilizing the output from a programmable arbitrary wave form generator (Wavetek Model 175) into a fast power supply/amplifier (Kepco Model BOP 36-6M; rise time for the current is 5×10^5 A/sec). The actual current profiles imposed on the cells were measured across a shunt using a storage digital oscilloscope (Nicolet 410). The sampling rate was at 5 msec. Figure 3 shows a typical recorded profile for current. The recorded profiles were then used to calculate the net time-averaged current (I_{ave}). The cells were initially brought to ~50% state of charge (~ 470 psi) by charging or discharging at 5A and then allowed to equilibrate for a minimum of 2 hours before starting the experiment. Two current profiles corresponding to 490 W and 430 W S/C loads were used at a period of 3 sec/cycle (10 RPM on the S/C)². For comparison, the cells were also charged at the equivalent time-averaged constant current of the simulation. The temperatures chosen were 0°C and -15°C corresponding to the most probable and the lowest expected temperatures, including margin, respectively.

²This is the baseline S/C spin rate required for attitude control. Other experiments have shown that the spin rate has minimal effect on the charging efficiency.

The cell pressure and voltage were monitored during the run. The strain gage was calibrated at each temperature by charging the cells to various pressures followed by discharging to 1.0V cutoff to get the corresponding available capacity. The charge/discharge rate of 5A was used to have a minimal thermal effect and to correspond to the approximate rate used during the deployment phase. Figure 4 shows the typical results for capacity versus cell pressure. These data can be fit to an equation of the form:

$$\text{Capacity (available)} = A + BP \quad (a)$$

where P is the cell pressure and A and B are constants. The charging efficiency, F, by definition is given by:

$$F = \frac{\text{Capacity(available)}}{\text{Capacity(input)}} \quad (b)$$

The Capacity(input) is simply the time-averaged current multiplied by the time, i.e., $I_{ave}t$. Therefore the instantaneous charging efficiency, F_t , becomes:

$$F_t = \frac{d}{dt} \left(\frac{A + BP}{I_{ave}t} \right) = \frac{B}{I_{ave}} \left(\frac{dP}{dt} \right) \quad (c)$$

Thus, the instantaneous charging efficiency is the first derivative of the curve of cell pressure vs. time multiplied by B/I_{ave} .

A typical curve of the change in cell pressure with time is shown in Fig. 5. The curve is rather noisy on a micro scale due to the cyclic nature of the current. Consistent, reliable results were obtained by curve fitting the pressure - time data using TableCurve³ software with F-statistics as the selection criteria. Figure 6(a) illustrates the typical goodness-of-fit between the equation and the data. The fit is excellent as evidenced by the extremely low values in the percentage residual ($< 2\%$) as shown in Fig 6(b). Similar fits were obtained for all the data using the equation of the form:

$$P = C + Dt + Et^3 \quad (d)$$

where C, D and E are constants. Combining equations (c) and (d) the instantaneous charging efficiency, F_t , becomes :

$$F_t = \left(\frac{B}{I_{ave}} \right) (D + 3Et^2) \quad (e)$$

Fitted curves under various test conditions of S/C power, ambient temperature and

³TableCurve, Jandel scientific, Corte Madera, CA.

increasing state of charge are illustrated by the plots in Figs. 7 to 11. For comparison, the charge efficiency under conditions of time-averaged constant charge current at similar S/C power and temperature are also presented.

RESULTS AND DISCUSSION

The AT&T S/C design rules require that the battery must not be discharged more than 70% based on a planning estimate of 58 AH total capacity; this corresponds to 17 AH remaining. It was expected that the batteries would be injected into transfer orbit at 85% state of charge⁴ or 49 AH available. The charging efficiency for the 430 W and 490 W S/C loads with sequential charging at 0°C and -15°C are shown in Figs. 7 and 8 respectively for available capacity ranging from 20 to 50 AH. These results indicate that:

- the charging efficiency is greater than 95% in most of the range tested, dropping to 92% at 0°C, 490 W at the 49 AH point expected during planning.
- the charging efficiency decreases with increasing state of charge of the cell and the decrease is more dramatic at 0°C than at -15°C.
- the charging efficiency is higher for 430 W than for 490 W.
- the charging efficiency is higher at lower temperatures due to increased oxygen overpotential as expected.

It must be emphasized that extrapolation of the curves beyond the data range is difficult particularly in the higher state of charge ranges. Note that these cells have nearly 70 AH capacity (c.f. Fig. 4) compared to their 50 AH nameplate capacity as do the TELSTAR 4 cells. Thus, the available capacity levels estimated in planning should be accomplished at reasonable efficiency. However, at the 490 W load, the time-averaged current is so low that it requires a significant amount of time to charge the battery. Thus it will be desirable to operate at lower loads such as 430 W as much as possible, or to utilize several powered down drift orbits to reach a sufficiently high state of charge prior to the deployment phase when no charging is possible.

The comparison of the charging efficiency between the simulations and the equivalent constant current charging is shown in Figs. 9 - 11. (Note that the equivalent constant current for the two cases are close but not identical to the time averaged simulation due to the difficulty in adjusting the programmable power supply. These differences, however, have a negligible effect on the results). In all cases, the constant current charging yields a slightly higher charging efficiency than the simulation. This can

⁴Not 100% due to self discharge on the launch pad and support of the S/C loads during ascent phase

be attributed to the following two factors. First the charging efficiency decreases non-linearly as the charging current is decreased while the time-averaged calculation assumes it to be linear so that the efficiency of the equivalent constant current could be either larger or smaller than that of the time averaged-current depending on whether the deviation of the efficiency from linearity is negative or positive. The other factor is that the simulation consists of both discharge and charge cycles, although the net time-averaged charge current is the same for the simulation as the constant current charging, the net charging efficiency of the simulation is always smaller than the constant current due to the fact that the discharging efficiency is always ~100% while the charging is not. Thus, the difference between the simulation and constant current charging will be determined by the sum of these two factors. The net result, however, is that suitably selected constant current charging can be used to determine the expected performance of the batteries for these conditions in qualification and acceptance testing. An example is given in Figure 12 to illustrate the charging efficiency of constant current charging as a function of both charging current and cell capacity available (state of charge).

SUMMARY

A sequential charging scheme for nickel hydrogen cells during transfer orbit of Telstar4 has been demonstrated to provide >90% charge efficiency necessary for a successful launch of the satellite. As expected, the charge efficiency is higher at lower ambient temperature of -15C and at a lower power load level of 430W. The charge efficiency using simulated conditions is slightly lower than charging at time averaged constant current. However, selected constant current charging can be used to determine the performance of these batteries for qualification and acceptance testing.

ACKNOWLEDGMENT

The authors wish to acknowledge the Martin Marietta Astro Space Telstar 4 Program Office for providing the experimental cells used in this study and to George Case for numerous helpful discussions. Appreciation is also extended to Linda Palmieri for providing the background data used in the simulation calculations.

LIST OF FIGURES

1. Transfer orbit array current at various rotational angles for a given load current.
2. Comparison of parallel and sequential charging method in terms of charging efficiency
3. Calculated and measured current profile for 490 W, 3 s/cycle, -15 C.
4. Calibration plot of capacity versus cell pressure at zero degree Celsius.
5. Plot of cell pressure variation with time at 490 W, 3 s/cycle simulation, 0 C
6. Plots showing (a) best fit line for the experimental data showing cell pressure change with time and (b) % Residuals for the fitted equation for data from experiment at 490 Watts, 3 s/cycle, 0 C.
7. Charging efficiency versus Capacity at 430 W and 460 W during 3 s/cycle simulation at 0 C.
8. Simulation of Charging efficiency versus Capacity at 430 W and 460 W, 3 s/cycle, 0 C
9. Comparison of simulation and constant current charging results at 430 W, 0 C
10. Plot of charging efficiency versus capacity under simulation and constant current conditions at 430 W, -15 C
11. Comparison of simulation and constant current charging at 490 W, -15 C
12. A 3-D presentation of charging efficiency as a function of charging current and cell capacity.

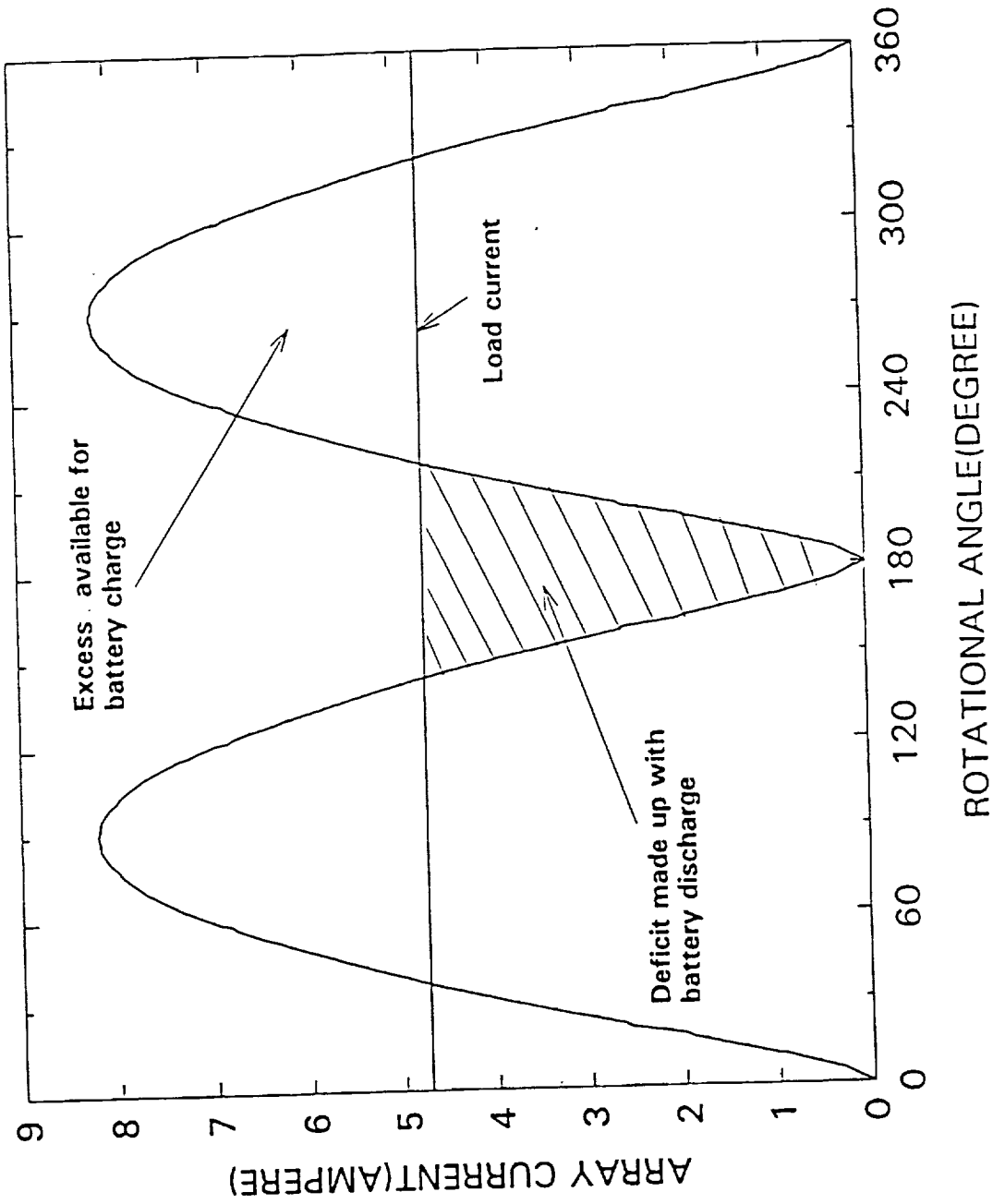


Fig.1 Transfer orbit array current at various rotational angles for a given load current

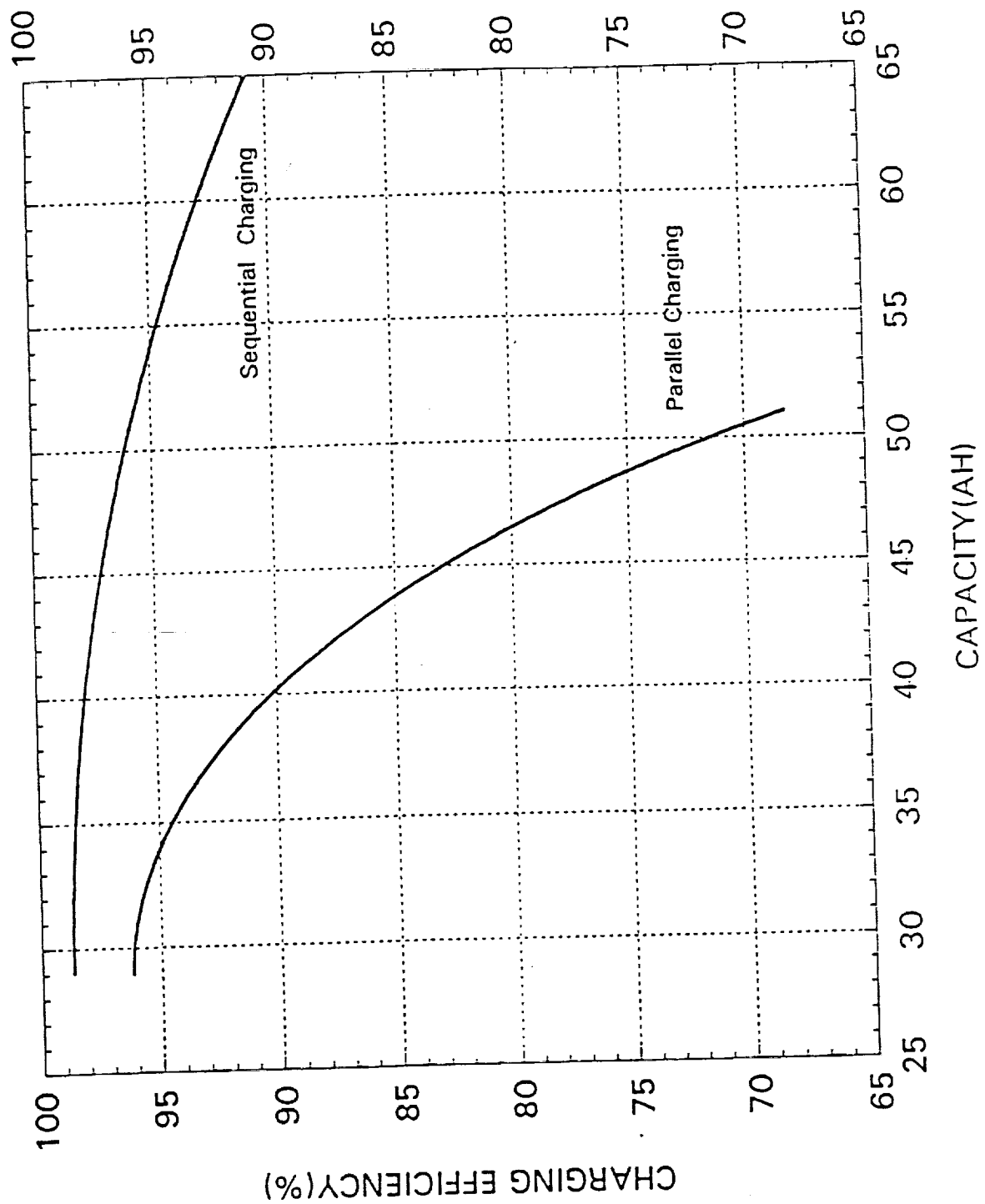


Fig.2 Comparison of parallel and sequential charging method in terms of charging efficiency 430W, 3sec/cycle, 0°C.

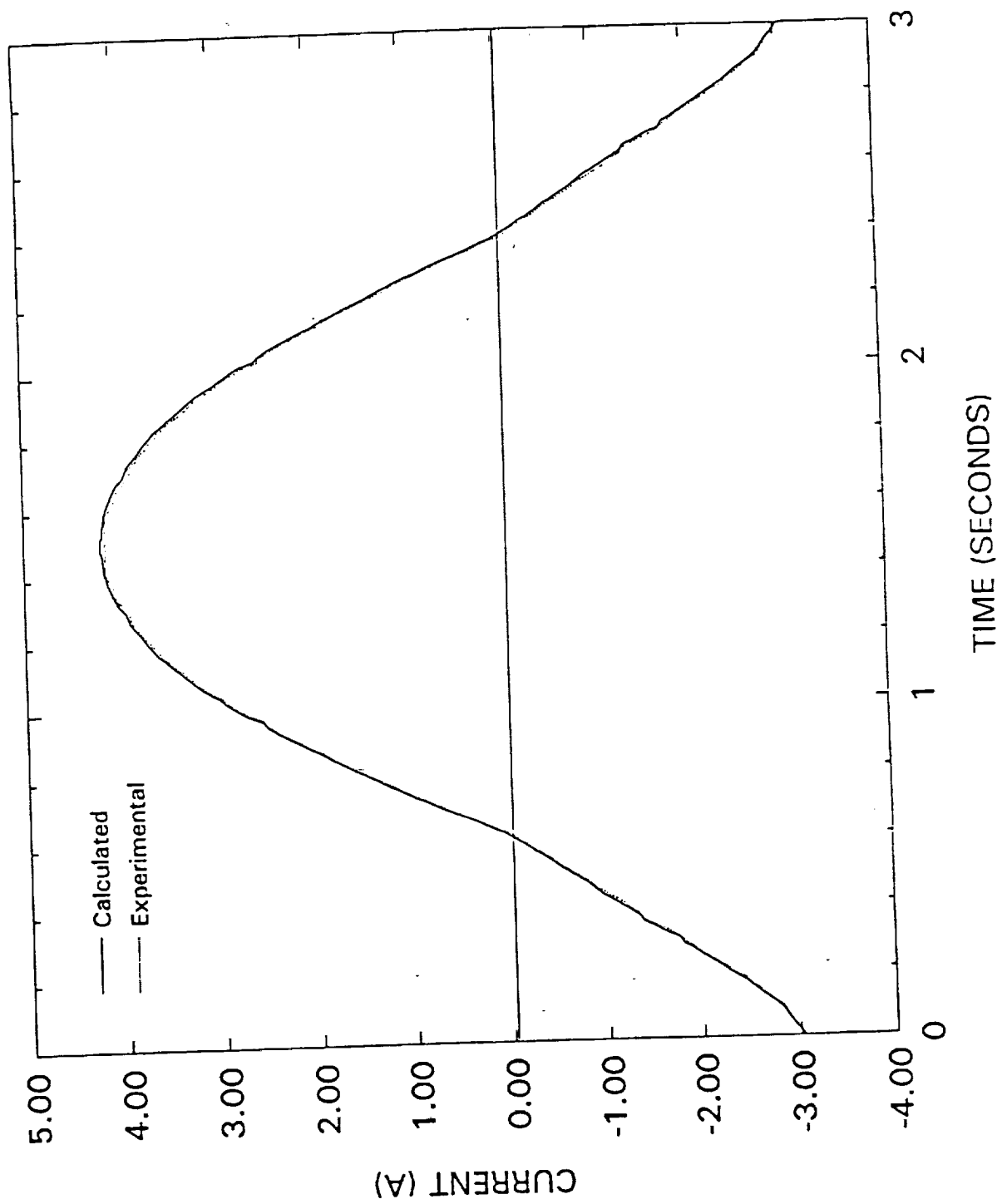


Fig.3. Calculated and measured current profile for 490 W, 3 sec/cy, -15C.

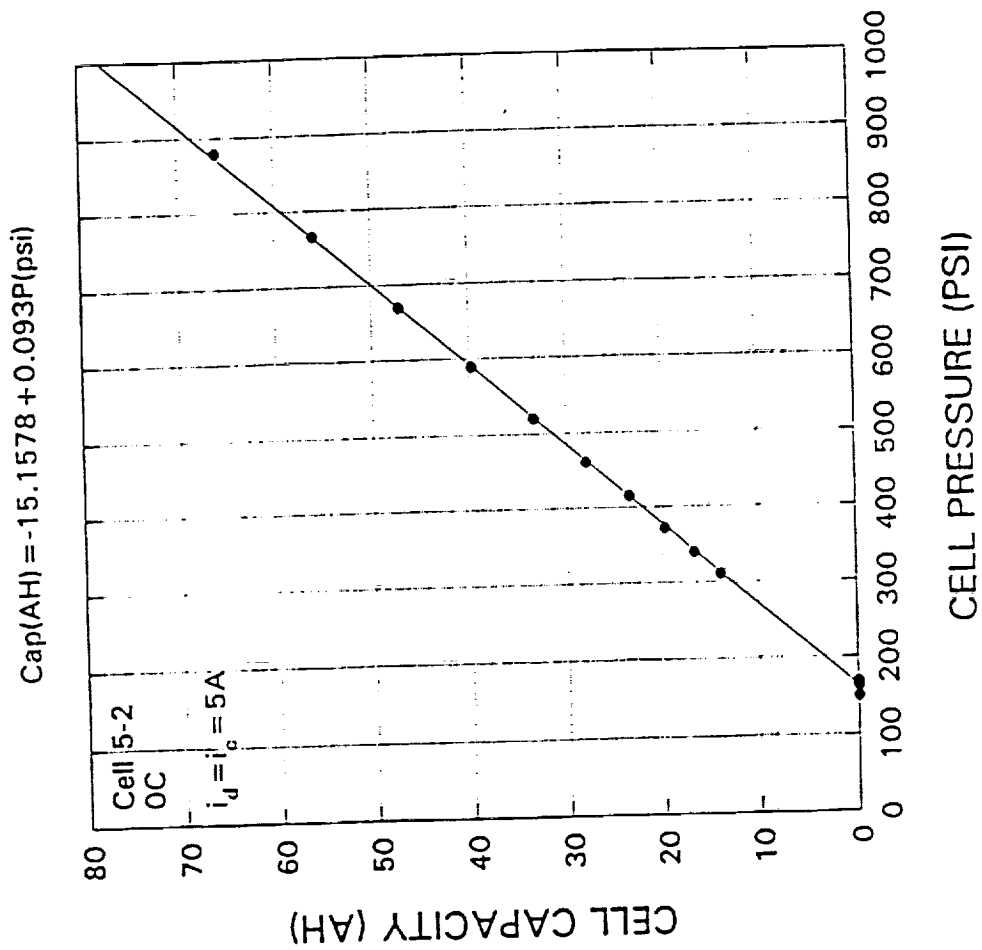


Fig.4 Capacity-pressure calibration curve

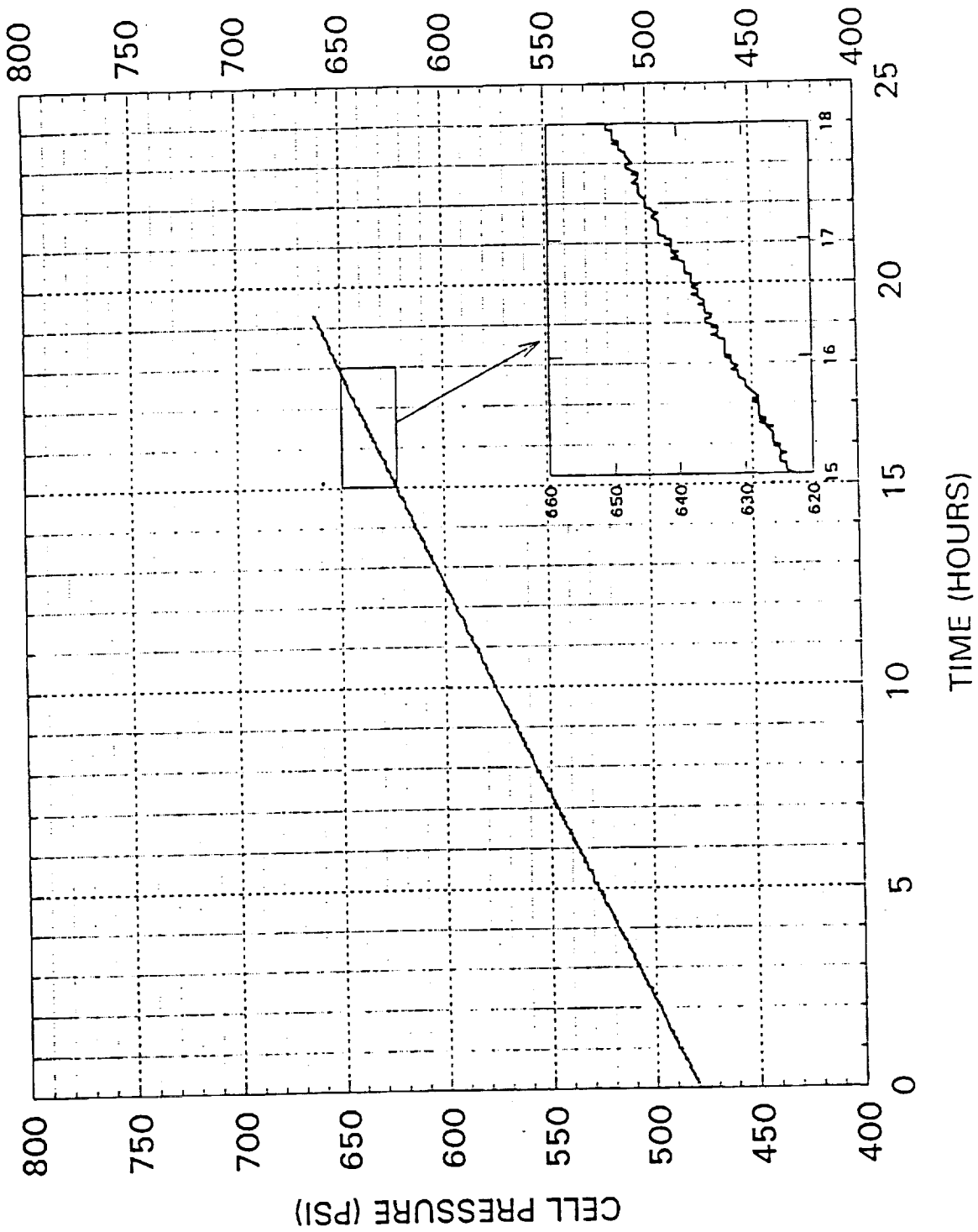
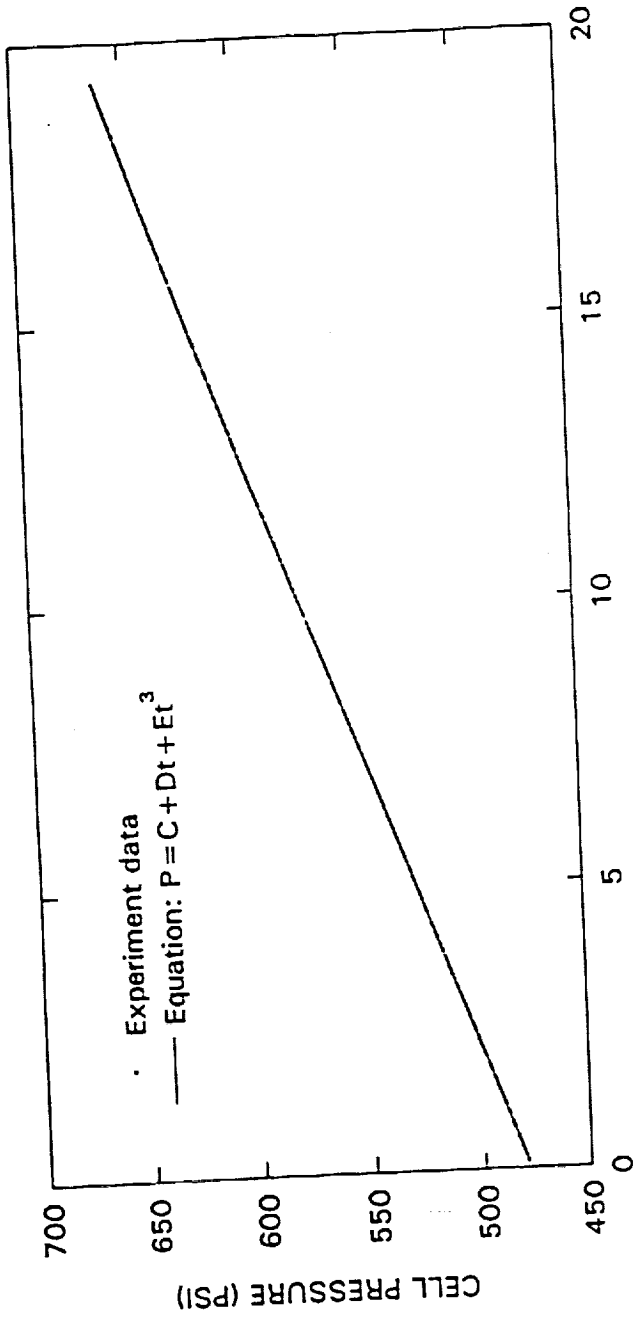
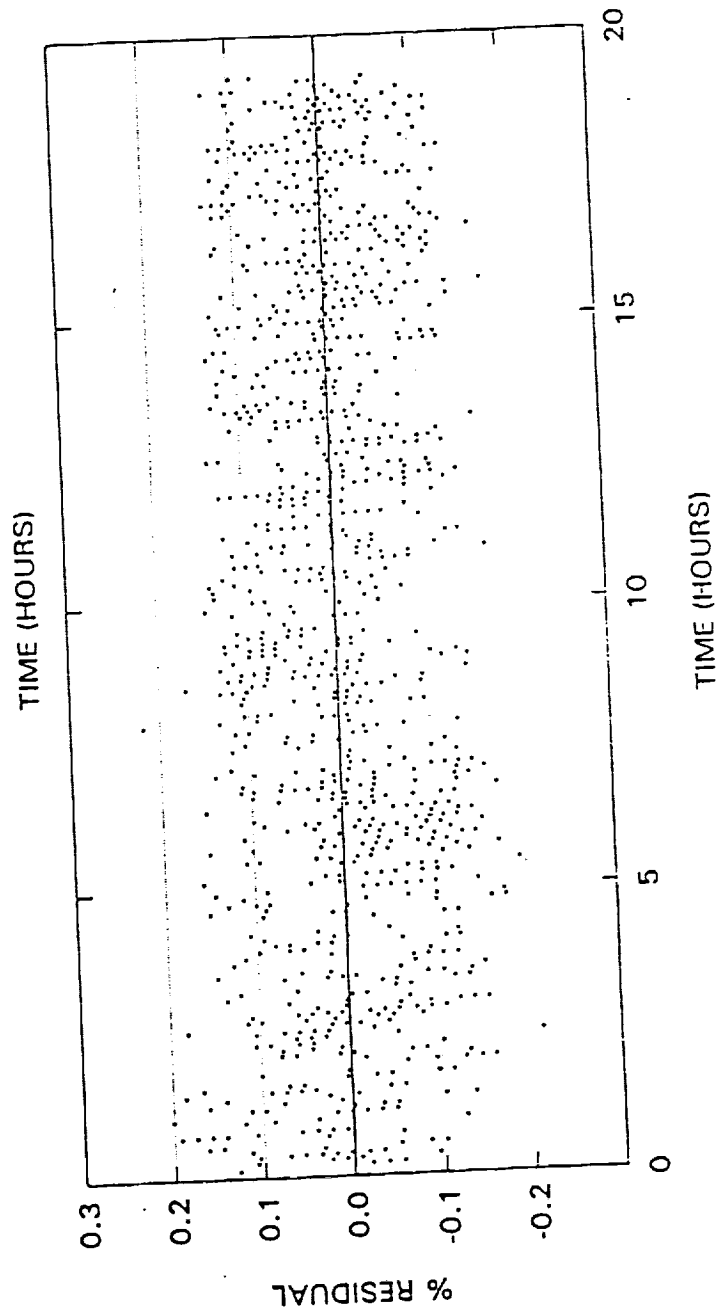


Fig.5 Cell pressure vs.time plot for 490W load, 3sec/cycle simulation, 0°C



(a)



(b)

Fig. 6 (a) Experimental data with equation fit (b) % residual of equation fit
490W, 3sec/cy, 0°C

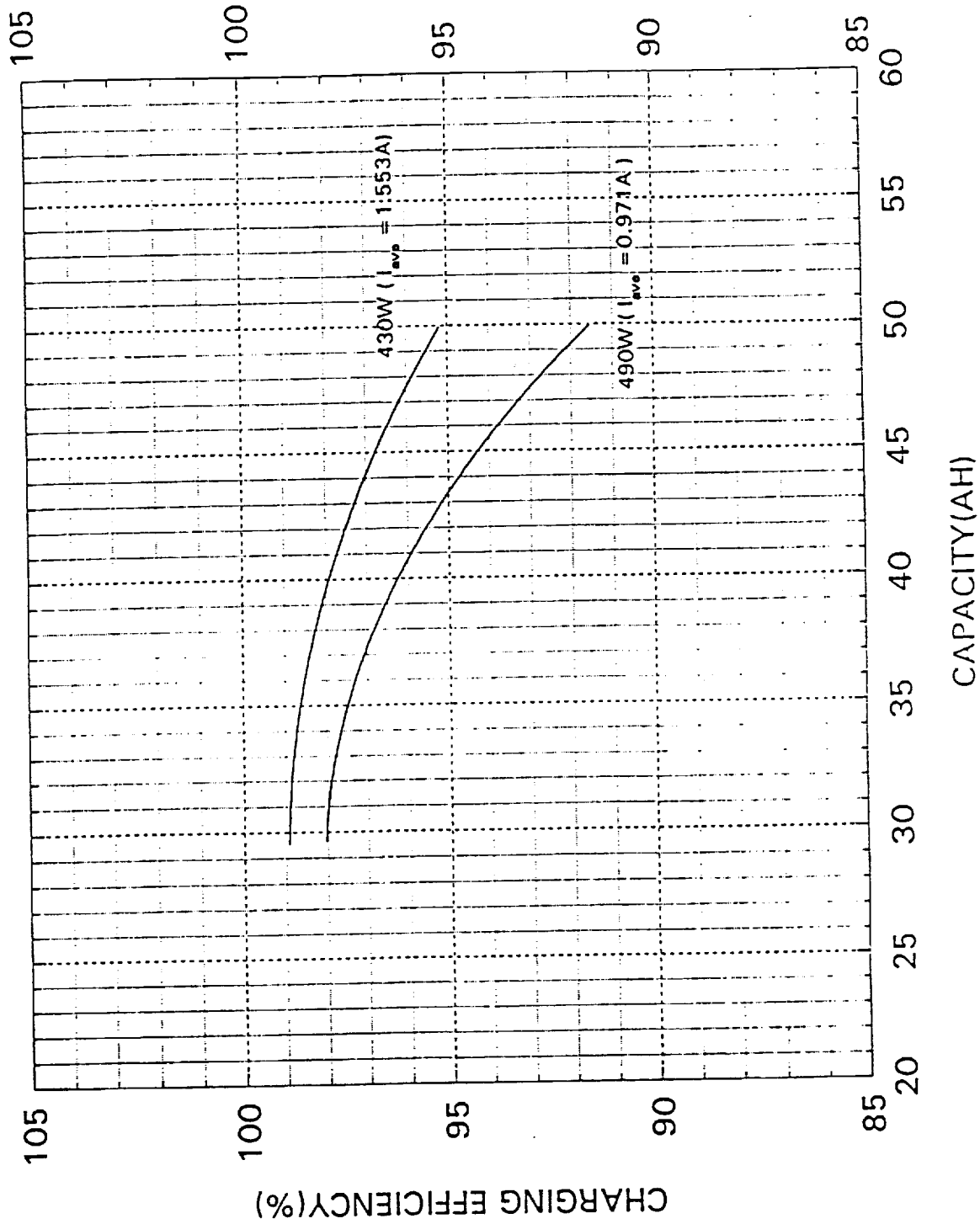


Fig.7 Charging efficiency vs. capacity for 430W and 490W loads. 3sec/cycle simulation, 0°C

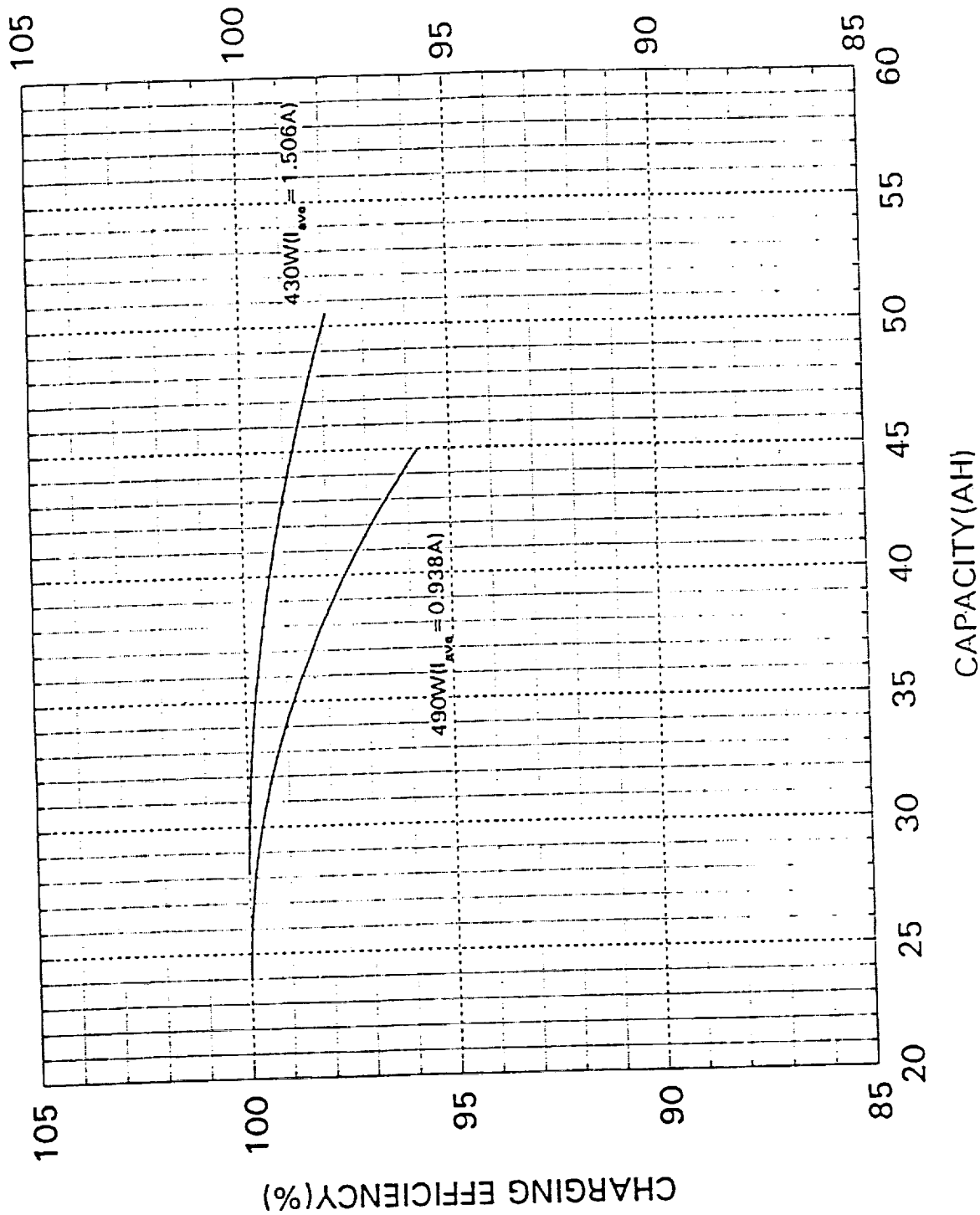


Fig. 8 Charging efficiency vs. capacity for 430w and 490w lods. 3sec/cycle simulation, -15°C

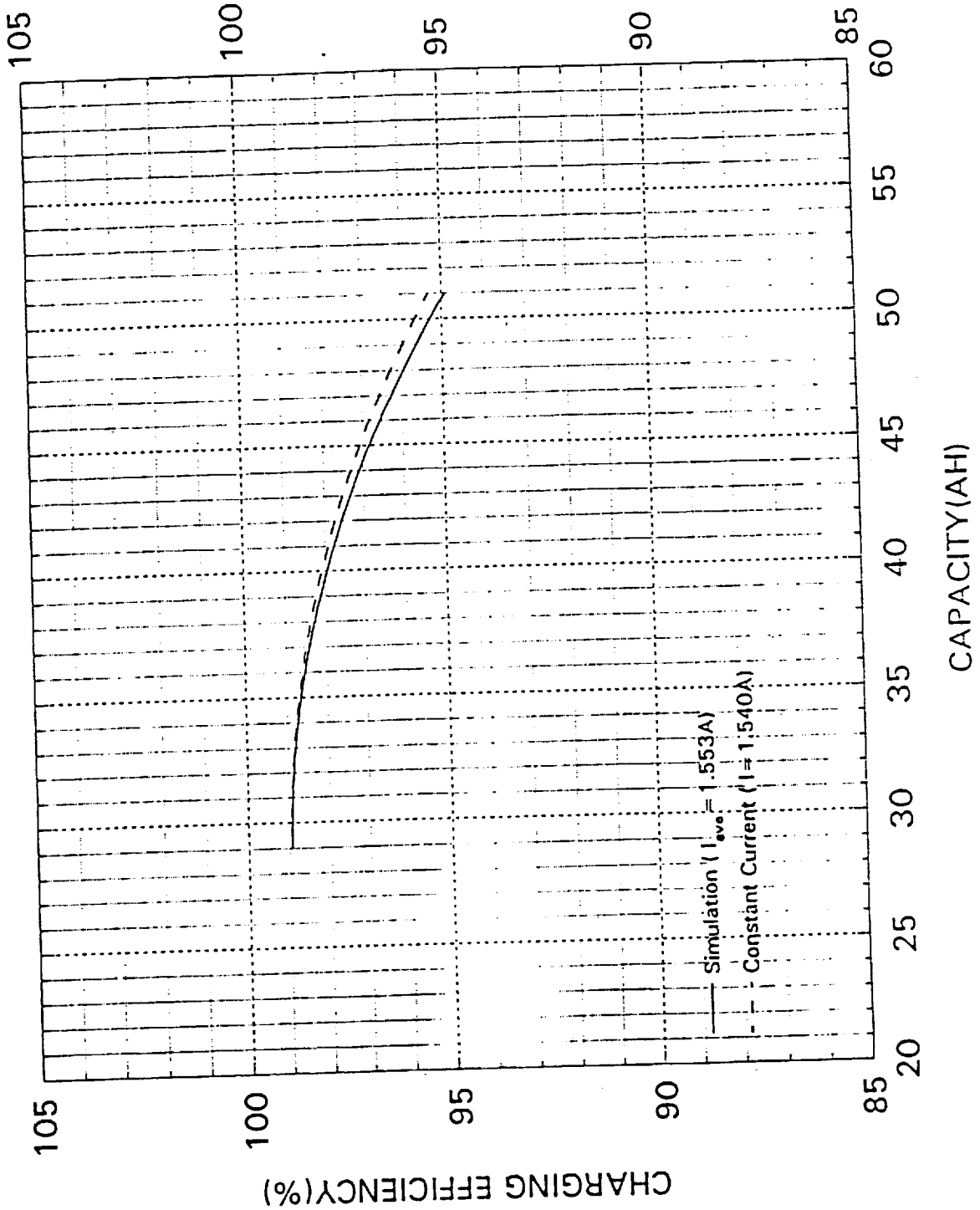


Fig.9 Comparison of simulation and constant current charging. 430W, 0°C

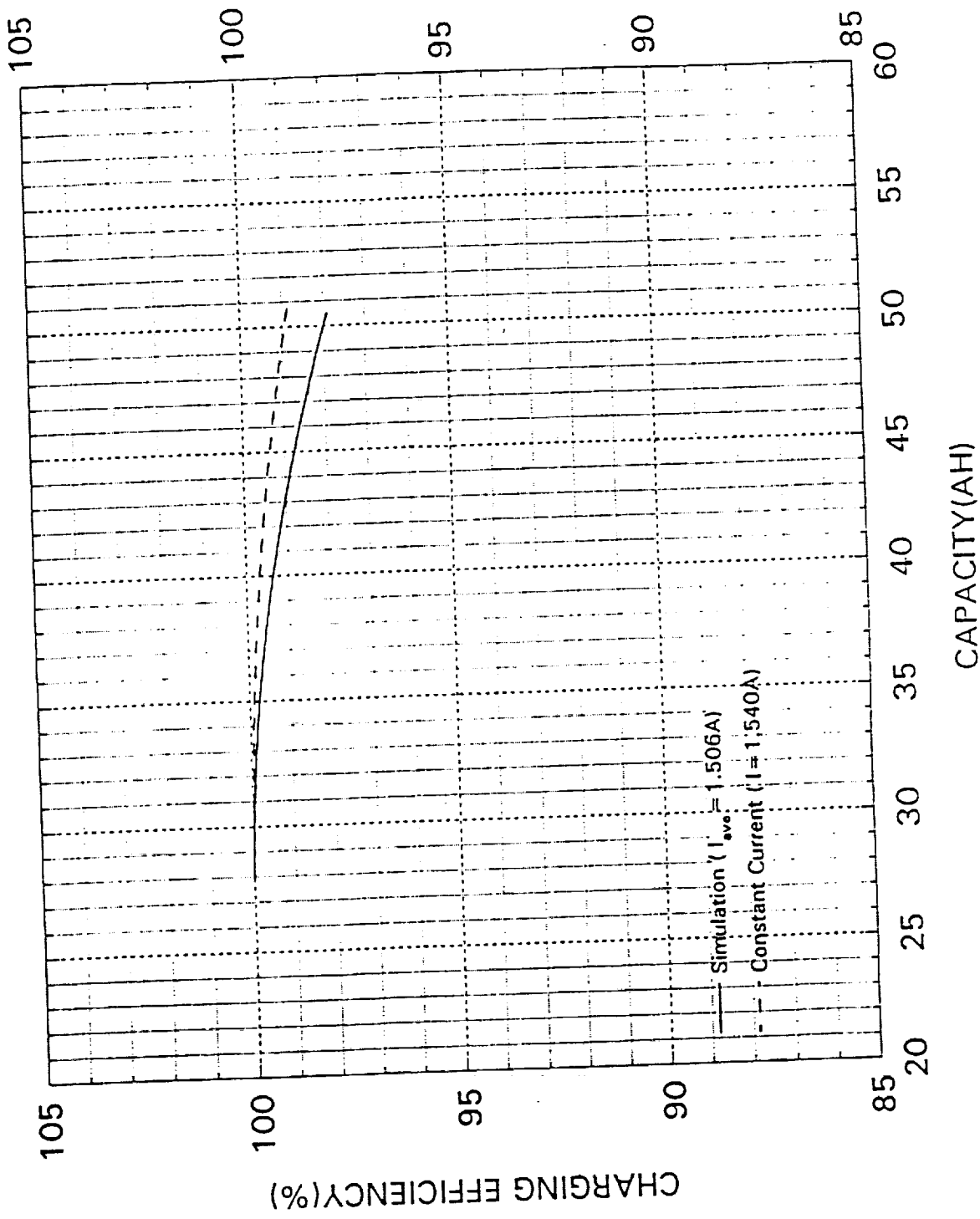


Fig.10. Comparison of simulation and constant current charging. 430W, -15°C

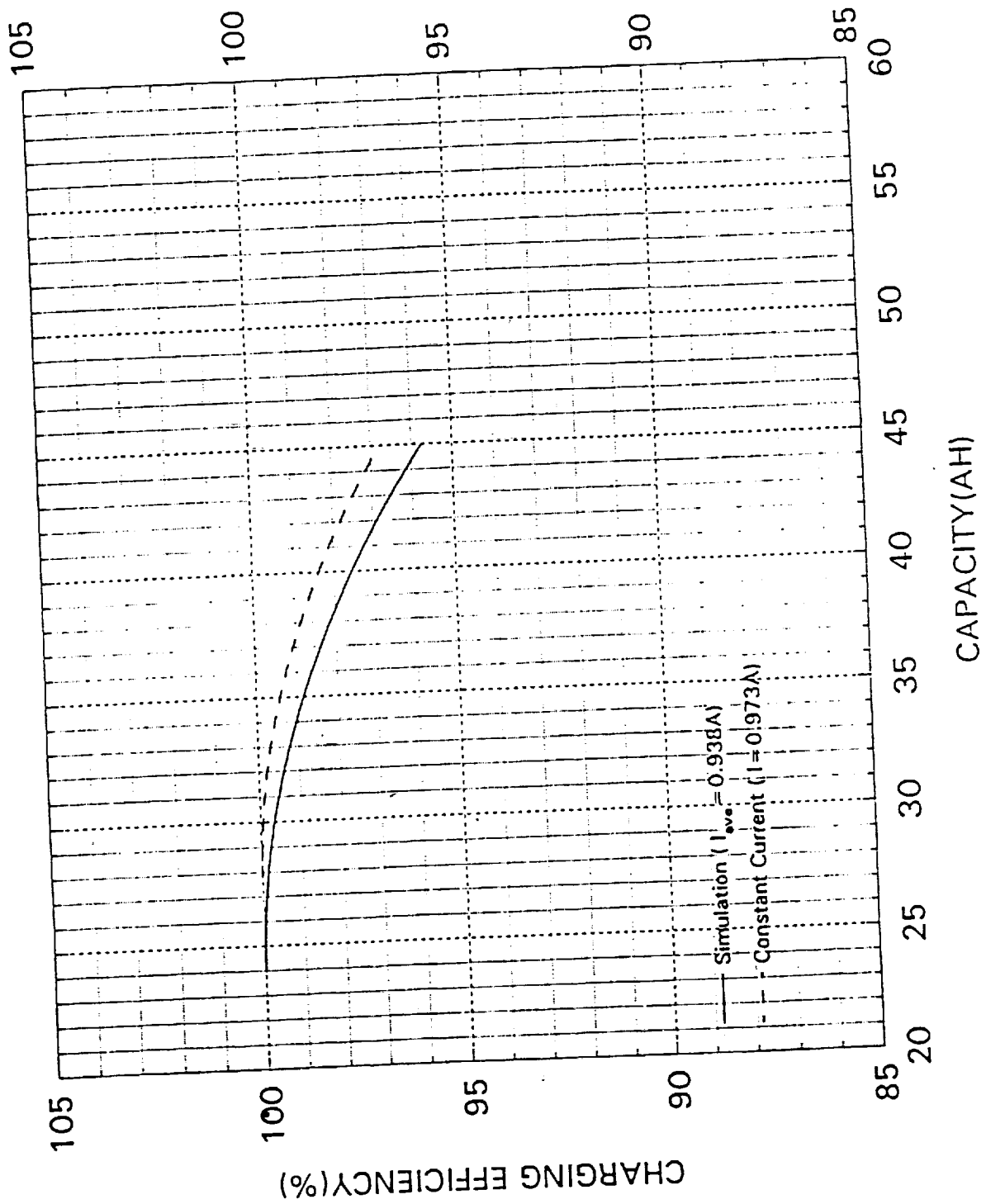


Fig.11. Comparison of simulation and constant current charging. 490W, -15°C

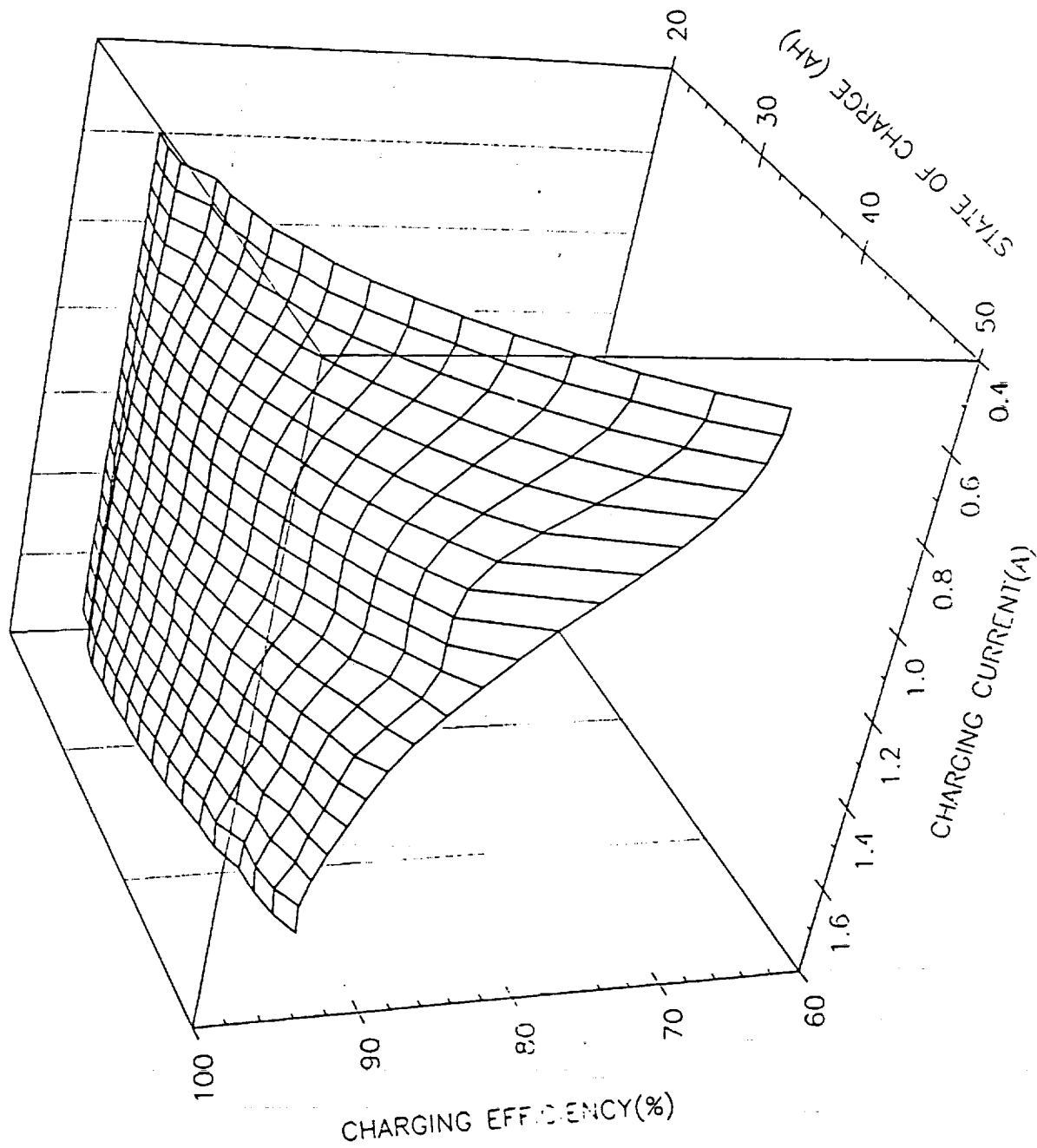


Fig.12 A 3--D presentation of charging efficiency as a function of charging current and cell capacity at 0°

Nickel-Cadmium Technologies Session

*Session Organizer: Patricia O'Donnell
NASA Lewis Research Center*

